

1 **Time series analysis of daily data of COVID-19 reported cases in Japan from**

2 **January 2020 to February 2023**

3 Ayako Sumi*

4 Division of Physics, Department of Liberal Arts and Sciences, Center for Medical

5 Education, Sapporo Medical University, Sapporo, Hokkaido 060-8556, Japan

6

7 * Corresponding author

8 E-mail: sumi@sapmed.ac.jp

9

10 **Abstract**

11 This study investigated temporal variational structures of the COVID-19
12 pandemic in Japan using a time series analysis incorporating maximum entropy method
13 (MEM) spectral analysis, which produces power spectral densities (PSDs). This method
14 was applied to daily data of COVID-19 cases in Japan from January 2020 to February
15 2023. The analyses confirmed that the PSDs for data in both the pre- and post-Tokyo
16 Olympics periods show exponential characteristics, which are universally observed in
17 PSDs for time series generated from nonlinear dynamical systems, including the so-called
18 susceptible/exposed/infectious/recovered (SEIR) model, well-established as a
19 mathematical model of temporal variational structures of infectious disease outbreaks.
20 The magnitude of the gradient of exponential PSD for the pre-Olympics period was
21 smaller than that of the post-Olympics period, because of the relatively high complex
22 variations of the data in the pre-Olympics period caused by a deterministic, nonlinear
23 dynamical system and/or undeterministic noise. A 3-dimensional spectral array obtained
24 by segment time series analysis indicates that temporal changes in the periodic structures
25 of the COVID-19 data are already observable before the commencement of the Tokyo
26 Olympics and immediately after the introduction of mass and workplace vaccination
27 programs. Lessons from theoretical studies for measles control programs may be
28 applicable to COVID-19.

29

30 **Introduction**

31 Since December 2019, a novel coronavirus designated as Severe Acute
32 Respiratory Syndrome Coronavirus 2 (SARS-CoV-2) has rapidly spread around the world,

33 affecting millions of people worldwide; its impact continues today. Waves of cases of
34 this novel coronavirus disease, also known as COVID-19, still occur recursively, although
35 these waves may well be prevented, and possibly eradicated, in the future. Considerable
36 effort to prevent and eradicate COVID-19 has been expended through COVID-19
37 surveillance, vaccinations, and theoretical and experimental research [1-4]. Among these
38 efforts, attempts to elucidate the mechanism of the COVID-19 pandemic have been of
39 great interest. Recently, researchers have tried to interpret the behavior of the pandemic
40 in terms of deterministic chaos [5-7]. Sapkota et al., reported that the hosting of the Tokyo
41 Olympic Games in Japan between 23 July and 8 August 2021 affected the mechanism of
42 the COVID-19 pandemic in the country [8]. Therefore, the temporal variational structures
43 of the data before and after the Olympic Games may differ, and examining this point is
44 significant from the standpoint of predicting the COVID-19 pandemic. However, typical
45 approaches cannot fully elucidate the temporal variational structures of the patterns of the
46 pandemic. This is because the data lengths of reported cases of COVID-19 are very short:
47 in Japan, the data are collected daily, and the number of data points was slightly above
48 1000 points by February 2023. Thus, a superior and powerful method of time series
49 analysis to elucidate the temporal variational structure of time series of even short data
50 length is required. In previous publications [9-11], we proposed a method that enables us

51 to analyze the time series of COVID-19 cases. In the present study, this method was
52 applied to examining the temporal variational structures of daily time series data of
53 reported COVID-19 cases for the entire country of Japan. Quantitative elucidations of the
54 COVID-19 pandemic are of great significance in epidemiology, and will contribute to the
55 development of surveillance of the disease.

56

57 **Methods**

58 **Data**

59 The present study analyzed daily data of reported COVID-19 cases for the entire
60 country of Japan from 16 January 2020 to 21 February 2023 (1133 data points). During
61 this period, a total 32,851,731 cases of COVID-19 were reported in Japan. The data used
62 in the present study were obtained from the Japan Ministry of Health, Labour, and
63 Welfare COVID-19 Data [12]. The data are indicated in S1 Dataset.

64

65 **Time series analysis**

66 We used a time series analysis consisting of maximum entropy method (MEM)
67 spectral analysis in the frequency domain and least squares method (LSM) in the time
68 domain [9-11,13,14]. The MEM is considered to have a high degree of resolution of
69 spectral estimates compared with other analysis methods of infectious disease

70 surveillance data such as the fast Fourier transform algorithm and autoregressive methods,
71 which require time series of long data lengths [15, 16]; therefore, an MEM spectral
72 analysis allows us to precisely determine short data sequences, such as the infectious
73 disease surveillance data used in this study [9-11,13-15].

74

75 **MEM spectral analysis**

76 We assumed that the time series data $x(t)$ (where t is time) were composed of
77 systematic and fluctuating parts [17]:

$$78 \quad x(t) = \text{systematic part} + \text{fluctuating part.} \quad (1)$$

79 To investigate temporal patterns of $x(t)$ in the monthly time series data, we performed
80 MEM spectral analysis [9-11,13,14]. MEM spectral analysis produces a power spectral
81 density (PSD), from which we obtain the power representing the amount of amplitude of
82 $x(t)$ at each frequency (note the reciprocal relationship between the scales of frequency
83 and period). The MEM-PSD, $P(f)$ (where f represents frequency), for the time series
84 with equal sampling interval Δt , can be expressed by

$$85 \quad P(f) = \frac{P_m \Delta t}{\left| 1 + \sum_{k=-m}^m \gamma_{m,k} \exp[-i2\pi fk\Delta t] \right|^2}, \quad (2)$$

86 where the value of P_m is the output power of a prediction-error filter of order m and $\gamma_{m,k}$

87 is the corresponding filter order. The value of the MEM-estimated period of the n th peak
88 component T_n ($=1/f_n$; where f_n is the frequency of the n th peak component) can be
89 determined by the positions of the peaks in the MEM-PSD.

90

91 **Least squares method**

92 The validity of the MEM spectral analysis results was confirmed by calculating
93 the least squares fitting (LSF) curve pertaining to the original time series data $x(t)$ with
94 MEM-estimated periods. The formula used to generate the LSF curve for $X(t)$ was as
95 follows:

$$96 \quad X(t) = A_0 + \sum_{n=1}^N A_n \cos\{2\pi f_n (t + \theta_n)\}. \quad (3)$$

97 The above formula is calculated using the LSM for $x(t)$ with unknown parameters f_n , A_0
98 and A_n ($n = 1, 2, 3, \dots, N$), where f_n ($= 1/T_n$; T_n is the period) is the frequency of the n -th
99 component; A_0 is a constant that indicates the average value of the time series data; A_n is
100 the amplitude of the n -th component; θ_n is the phase of the n -th component; and N is the
101 total number of components. The reproducibility level of $x(t)$ by the optimum LSF curve
102 was evaluated via a Spearman's rank correlation (ρ) analysis performed using SPSS
103 (Statistical Package for the Social Sciences) version 17.0J software (SPSS, Tokyo, Japan).
104 A p value of ≤ 0.05 was considered statistically significant.

105

106 **Results**

107 **Temporal Variations in COVID-19 Reported Cases Data**

108 Daily data of reported cases of COVID-19 from 16 January 2020 to 21 February
109 2023 in Japan are plotted in Fig 1a. A closer view of the data from January 2020 to June
110 2021 is illustrated in Fig 1b, which shows four large waves observed at intervals of about
111 four to five months, peaking in April and July 2020, and January and May 2021.
112 Subsequently, Fig 1a shows four large waves at longer intervals than before,
113 approximately five to six months, with peaks in August 2021, February and August 2022,
114 and January 2023.

115

116 **Fig 1. Daily data of COVID-19 reported cases of Japan from 16 January 2020 to 21**
117 **February 2023.** (a) The original data. (a') Histogram of the original data. (b)
118 Enlargement of the original data from 16 January 2020 to 30 June 2023. (c) The
119 logarithm-transformed data of the original data (thin line) and its optimum LSF curve
120 (bold line). (d) MEM-PSD of the residual data in the low-frequency range ($f \leq 1.2$). (e)
121 The residual data obtained by subtracting the LSF curve from the log-data. (e') Histogram
122 of the residual data. Small vertical line in *e* indicates the boundary of phase I (pre-Tokyo
123 Olympic Games, 11 February 2020–22 July 2021) and phase II (post-Tokyo Olympic

124 Games, 23 July 2021–21 February 2023).

125

126 **Preparing the data for analysis**

127 We take the reported cases data $x(t)$ (t : time) to represent discrete ones at $t = k\Delta t$ ($k =$
128 $1, 2, 3, \dots, N$) where Δt is the time interval and N the length of the time series ($\Delta t = 1$ -day
129 and $N = 1133$, in the present study). Fig 1a' gives the frequency histogram for $x(t)$ (Fig
130 1a). This histogram is apart from the normal distribution required for conventional
131 spectral analysis. Then, we introduced the logarithm transformation of $x(t)$ (Fig 1a).
132 Because the data from 16 January to 10 February 2020 include 17 zero values and are not
133 available for the logarithm transformation, the 15 cases that were reported during this
134 period are ignored and the starting point of the data was re-set to 11 February 2020. As a
135 result, the present study uses the data from 11 February 2020 to 21 February 2023. For
136 the data in this period, the logarithm-transformed data is shown in Fig 1c, where the
137 spikiness of the reported cases observed in $x(t)$ has been reduced, and a long-term
138 decreasing trend is observed.

139 To remove the long-term trend of the log-data shown in Fig 1c, PSD, $P(f)$ (f :
140 frequency), for the log-data was calculated, and the PSD ($f \leq 1.2$) is displayed in Fig 1d
141 (unit of f : 1/year). Therein, the longest period can be observed as the prominent peak at

142 the position of 5.3-year period. With this 5.3-year period, we modeled the long-term trend
143 in the COVID-19 pandemic by calculating the LSF curve (Equation (3)) for the entire
144 log-data (Fig 1c). The LSF curve obtained (Fig 1c) expresses the long-term trend of the
145 log-data well.

146 We removed the LSF curve from the log-data (Fig 1c), and the residual time series
147 data were obtained, as shown in Fig 1e. The frequency histogram for this residual data is
148 shown in Fig 1e' and approximates to the normal distribution required for conventional
149 spectral analysis. Normality of distribution was assessed using the χ^2 fitting test, and the
150 null hypothesis was not rejected ($P = 0.76$).

151

152 **Power spectral density of the time series data**

153 To investigate the effect of hosting the Tokyo Olympic Games on the temporal
154 variational structures of the COVID-19 pandemic in Japan, the residual data (Fig 1e) were
155 divided into two ranges (phases I and II) in accordance with the starting and ending points
156 of the Tokyo Olympic Games (23 July 2021 and 8 August 2021, respectively): pre-
157 Olympic Games (11 February 2020 – 22 July 2021) for phase I and post-Olympic Games
158 (23 July 2021 – 21 February 2023) for phase II. MEM-PSDs for the residual data of
159 phases I and II were calculated. The semi-log plots of the PSD are shown in Fig 2a and

160 2b for phases I and II, respectively.

161

162 **Fig 2. MEM-PSDs for two ranges of the residual data ($f < 30.0$).** (a) Phase I (pre-

163 Tokyo Olympic Games, 11 February 2020–22 July 2021). (b) Phase II (post-Tokyo

164 Olympic Games, 23 July 2021- 21 February 2023).

165

166 **Gradient of power spectral density**

167 As seen in the PSDs for phases I and II in Figs 2a and 2b, respectively, the overall

168 trend of each PSD indicates the exponential form

$$169 \quad P(f) : \exp(-\lambda f) \quad (4)$$

170 until the PSDs level off at the lowest limit determined by the accuracy of the present data,

171 that is, the number of significant digits in the data. The values of λ for phases I and II are

172 0.25 and 0.28, respectively.

173

174 **Dominant spectral lines**

175 Close-ups of the low-frequency regions of the PSDs in Figs 2a and 2b are shown

176 in Figs 3a and 3b, respectively. For phase I (Fig 3a), the dominant spectral peak is

177 observed at $f=2.8$, corresponding to a 0.36-year (4.3-month), with considerably large

178 powers representing the amplitude of $x(t)$ at each frequency. For phase II (Fig 3b), the

179 dominant spectral peak is observed at $f = 2.0$, corresponding to a 0.50-year (6.0-month),
180 with considerably large powers.

181

182 **Fig 3. Close-up of the low-frequency region ($f < 4.0$) in Figs 2a and 2b:** (a) Phase I
183 (pre-Tokyo Olympic Games, 11 February 2020–22 July 2021). (b) Phase II (post-
184 Tokyo Olympic Games, 23 July 2021–21 February 2023).

185

186 **Segment time series analysis**

187 Periodic structures of the residual data were further investigated via segment
188 time series analysis (Fig 1e). The residual data (Fig 1e) are divided into multiple segments,
189 and the PSD is calculated for each segment. In this study, each segment represents the
190 time interval of 365 days, and the starting point of two consecutive segments is delayed
191 by six days. The PSDs thus obtained are shown as a 3D spectral array in Fig 4. In the 3D
192 spectral array, the power is plotted against the frequency (horizontal axis) and time (right
193 vertical axis). In the frequency range of $1.0 < f < 4.0$, corresponding to the periods of 3.0
194 months to 1 year, spectral lines are clearly observed over the whole time range.

195 The temporal variations of the frequency of dominant spectral lines observed in
196 the 3D spectral array (Fig 4) are plotted in Fig 5. As seen in the figure, spectral peaks

197 were observed around $f = 3.0$ (0.33 year) before May 2021. After May 2021, and
198 beginning before the Tokyo Olympic Games started in July 2021, spectral peaks
199 gradually migrated to the low-frequency range, and were observed to be around $f = 2.2$
200 from July to November 2021, and then remained relatively constant around $f = 2.0$
201 thereafter.

202

203 **Fig 4. Three-dimensional spectral array for the residual data in the frequency range**
204 **of $1.0 \leq f \leq 10.0$.**

205

206 **Fig 5. Temporal variations of the frequencies of dominant spectral peaks detected**
207 **in the frequency range of $1.0 \leq f \leq 4.0$.**

208

209 **Discussion**

210 The most notable result obtained in the present study is that, as observed in Fig
211 5, the gradual migration of the spectral line to the low-frequency range from 3.0 (0.33-
212 year) to 2.0 (0.5-year) during May to July 2021 is already observable before the
213 commencement of the Tokyo Olympic Games in July 2021 and immediately after the
214 introduction of mass and workplace vaccination programs in April 2021, at a time when
215 Japan's vaccination rate was 4%. The vaccine rate increased quickly from May; the

216 maximum number of daily inoculations was 1.6 million. By October 2021, more than 77
217 million people, equivalent to 61.8% of the targeted population, had completed the
218 vaccination series [18]. The temporal behavior of periodic structures observed in Fig 5
219 indicates that theoretical studies for measles control programs, based on predictions that
220 vaccination generates an increase in the inter-epidemic period (IEP), corresponding to the
221 interval between major waves of an epidemic, may also apply to COVID-19 [19,20]. The
222 IEP of measles epidemics has been investigated with time series analysis and
223 mathematical models [21-27]. The IEP represents the amount of time required to
224 accumulate a cohort of susceptible individuals that is sufficiently large to allow the
225 measles virus to effectively spread over a community once it is introduced from outside.
226 Our previous work investigated the IEP of measles epidemics in Japan and Wuhan in
227 China using the present method of spectral analysis [19,20], and confirmed that the IEP
228 increases as the vaccination ratio increases, as predicted by theoretical studies for a
229 mathematical model of temporal variational structures of infectious diseases [21,22,28].
230 Based on the theoretical studies of measles and our preceding work in that disease, the
231 present finding that period structures of the COVID-19 data of Japan changed temporally
232 after May 2021 may be the effect of the increased vaccination rate in the previous month,
233 April 2021.

234 With respect to the exponential characteristics of the PSDs for COVID-19 data
235 (Figs 2a and 2b), our preceding work clarified that the PSDs for the time series generated
236 from deterministic, nonlinear dynamical systems, such as the so-called
237 susceptible/exposed/infectious/recovered (SEIR) epidemic model [29] and the Rössler,
238 Lorenz and Duffing models [30,31], exhibit exponential characteristics. With respect to
239 infectious disease epidemics, preceding research has confirmed that exponential spectral
240 peaks are observed for incidence data of measles in Japan [15], Wuhan [19], New York
241 City [29] and several communities in Denmark, the UK and the USA [32], as well as for
242 chaotic and periodic time series generated by the SEIR epidemic model [29]. Thus, the
243 present finding of exponential characteristics of the PSDs for COVID-19 (Figs 2a and 2b)
244 suggests that the number of reported cases of COVID-19 in Japan is based on
245 deterministic nonlinear dynamics.

246 For the magnitude of the PSD gradient λ , we clarified in our preceding work that
247 λ decreases from the periodic state through the bifurcation process and reaches a
248 minimum in the chaotic state, based on our preceding work on the SEIR model [29] and
249 the Rössler model [30] throughout a series of period-doubling cascade through chaos.
250 The decrease of the magnitude of λ can be considered to be the result of fluctuations
251 mixed in a deterministic, nonlinear dynamical system [15]. With respect to the

252 fluctuations, two possibilities have been postulated by the author's group [15,30]; first,
253 the amplitude fluctuation could be generated by an instability due to the nonlinearity of
254 the system, as clarified in the result using the Rössler model, or the fluctuations could
255 result from undeterministic noise. In both cases, the magnitude of λ decreases because the
256 high-frequency components do not decline too rapidly [15,33]. In the present study, we
257 confirmed that the magnitude of λ for the pre-Olympics period is smaller than that of the
258 post-Olympics period. This result reflects the relatively high complex variations of the
259 data in the pre-Olympics period, which appears to support Sapkota et al.'s finding that,
260 among Japan's 47 prefectures, the number of prefectures exhibiting chaotic
261 characteristics was lower after the Tokyo Olympics than before [8]. A detailed study
262 investigating chaotic characteristics for each prefecture in Japan is the subject of a
263 forthcoming study.

264

265 **Conclusions**

266 In general, biological phenomena are both nonstationary and nonlinear, and
267 transit from one state to another in a complicated manner. Based on the results obtained
268 in the present study, the periodic structures of epidemics of infectious diseases, including
269 COVID-19, can be said to change over time. It is not appropriate to deal with the entirety

270 of an overall time series incorporating such states. Thus, for elucidating a temporal
271 evolution of nonlinear phenomena, it is preferable to deal with segments of time series of
272 shorter data length via segment time series analysis, as performed in the present study.
273 Investigation of temporal variational structures of disease epidemics with segment time
274 series analysis can be expected to contribute to long-term and effective COVID-19
275 control programs in Japan.

276 In conclusion, the following three results are confirmed in the present study: First,
277 the exponential characteristics of PSDs can be observed for the COVID-19 data of Japan
278 in both pre- and post-Olympics periods, which is peculiar to the nonlinear dynamical
279 process. Second, the magnitude of the gradient of exponential PSD for the pre-Olympics
280 period is smaller than that of the post-Olympics period, because of the relatively high
281 complex variations of the data in the pre-Olympics period caused by a deterministic,
282 nonlinear dynamical system and/or undeterministic noise. Third, changes in the periodic
283 structures of the COVID-19 data were already occurring before the Tokyo Olympic
284 Games began in July 2021 and immediately after the mass and workplace vaccination
285 programs were introduced in April 2021, indicating that the findings of theoretical studies
286 for measles control programs may also apply to the COVID-19 data.

287

288 **References**

- 289 1. Hu B, Guo H, Zhou P, Shi ZL. Characteristics of SARS-CoV-2 and COVID-19. *Nat*
290 *Rev Microbiol* 2021; 19: 141-154.
- 291 2. Zhang X, Lobinska G, Feldman M, Dekel E, Nowak MA, Pilpei Y, et al. A spatial
292 vaccination strategy to reduce the risk of vaccine-resistant variants. *PLoS Comput*
293 *Biol* 2022; 18: e1010391 (27 pages).
- 294 3. Rana R, Tripathi A, Kumar N, Ganguly NK. A comprehensive overview on COVID-
295 19: future perspective. *Front Cell Infect Microbiol* 2021; 11: 744903-744918.
- 296 4. Sharma A, Farouk IA, Lal SK. COVID-19: a review on the novel coronavirus disease
297 evolution, transmission, detection, control and prevention. *Viruses* 2021; 13: 202-226.
- 298 5. Bonasera A, Zhang S. Chaos, percolation and the coronavirus spread. *Front Phys*
299 2020; 8: 171-175.
- 300 6. Joens A, Strigul N. Is spread of COVID-19 a chaotic epidemic? *Chaos Solitons*
301 *Fractals* 2021; 142: 110376-110385.
- 302 7. Sapkota N, Murata A, Karwowski W, Davahli MR, Fiok K, Al-Juaid A, et al. The
303 Chaotic Behavior of the Spread of Infection During the COVID-19 Pandemic in the
304 United States and Globally. *IEEE Access* 2021; 9: 80692-80702.
- 305 8. Sapkota N, Murata A, Karwowski W, Davahli MR, Fiok K, Al-Juaid A, et al. The
306 Chaotic Behavior of the Spread of Infection during the COVID-19 Pandemic in Japan.
307 *Int J Environ Res Public Health* 2022; 19: 12804-12819.
- 308 9. Sumi A, Kobayashi N. Time-series analysis of geographically specific monthly
309 number of newly registered cases of active tuberculosis in Japan. *PLoS One* 2019; 14:
310 e0213856 (12 pages).
- 311 10. Mise K, Sumi A, Takatsuka S, Toyoda S. Associations between meteorological
312 factors and reported mumps cases from 1999 to 2020 in Japan. *Epidemiologia* 2021;
313 2: 162-178.
- 314 11. Ohtomo N, Kobayashi N, Sumi A, Ohtomo N. Relationship of cholera incidence to
315 El Niño and solar activity elucidated by time-series analysis. *Epidemiol Infect* 2010;
316 138: 99-107.
- 317 12. MHLW Visualizing the Data: Information on COVID-19 Infections. [(accessed on
318 28 February
319 2023)]. [https://covid19.mhlw.go.jp/public/opendata/newly_confirmed_cases_daily.c](https://covid19.mhlw.go.jp/public/opendata/newly_confirmed_cases_daily.csv)
320 [sv](https://covid19.mhlw.go.jp/public/opendata/newly_confirmed_cases_daily.csv).
- 321 13. Harigane K, Sumi A, Mise K, Kobayashi N. The role of temperature in reported
322 chickenpox cases from 2000 to 2011 in Japan. *Epidemiol Infect* 2015; 143: 2666-
323 2678.

- 324 14. Chen B, Sumi A, Wang A, Zhou W, Kobayashi N. Role of meteorological conditions
325 in reported chickenpox cases in Wuhan and Hong Kong, China. *BMC Infect Dis* 2017;
326 17: 538-546.
- 327 15. Sumi A, Ohtomo N, Tanaka Y, Koyama A, Saito K. Comprehensive spectral analysis
328 of time series data of recurrent epidemics. *Jpn J Appl Phys* 1997; 36: 1303-1318.
- 329 16. Ohtomo, N, Terachi, S, Tanaka, Y, Tokiwano, K, Kaneko, N. New method of time
330 series analysis and its application to Wolf's sunspot number data. *Jpn J Appl Phys*
331 1994; 33: 2321–2831.
- 332 17. Armitage, P, Berry, G. Matthews, J.N.S. *Statistical Methods in Medical Research*, 4th
333 ed.; Blackwell Science: Oxford, UK, 2012.
- 334 18. Mori H, Naito T. A rapid increase in the COVID-19 vaccination rate during the
335 Olympic and Paralympic Games 2021 in Japan. *Hum Vaccin Immunother* 2022; 18:
336 e2010440.
- 337 19. Luo T, Sumi A, Zhou D, Kamo K, Yu B, Zhao B, et al. Study on the effect of measles
338 control programmes on periodic structures of disease epidemics in a large Chinese
339 city. *Epidemiol Infect* 2010; 139: 257-264.
- 340 20. Sumi A, Kamo K, Ohtomo N, Kobayashi N. Study of the effect of vaccination on
341 periodic structures of measles epidemics in Japan. *Microbiol Immunol* 2007; 51: 805-
342 814.
- 343 21. Anderson RM, Grenfell BT. Oscillatory fluctuation in the incidence of infectious
344 disease and the impact of vaccination: time series analysis. *J Hyg, Cambridge* 1984;
345 93: 587–608.
- 346 22. Anderson RM, May RM. Directly transmitted infectious diseases: control by
347 vaccination. *Science* 1982; 215: 1053–1060.
- 348 23. Anderson RM, May RM. *Infectious Diseases of Humans: Dynamics and Control*.
349 London: Oxford University Press, 1991.
- 350 24. Clegg EJ. Infectious disease mortality in two Outer Hebridean islands: 1. Measles,
351 pertussis and influenza. *Ann Hum Biol* 2003; 30: 455–471.
- 352 25. Cliff A, Haggett P, Smallman-Raynor M. *Measles: A Historical Geography of a*
353 *Major Human Viral Disease from Global Expansion to Local Retreat, 1840–1992*.
354 Oxford: Blackwell, 1993.
- 355 26. Gomes MC, Gomes JJ, Paulo AC. Diphtheria, pertussis, and measles in Portugal
356 before and after mass vaccination: a time series analysis. *European Journal of*
357 *Epidemiol* 1999; 14: 791–798.
- 358 27. Grenfell BT, Bjornstad ON, Kappey J. Travelling waves and spatial hierarchies in
359 measles epidemics. *Nature* 2001; 414: 716–723.
- 360 28. Grenfell BT, Anderson RM. The estimation of age-related of infection from case
361 notifications and serological data. *J Hyg, Cambridge* 1985; 95: 419–436.

- 362 29. Sumi A, Ohtomo N, Tanaka Y. Study on chaotic characteristics of incidence data of
363 measles. *Jpn J Appl Phys* 1997; 36: 7460–7472.
- 364 30. Ohtomo N, Sumi A, Tanaka Y, Tokiwano K, Terachi S. A detailed study of power
365 spectral density for Rössler system. *J Phys Soc Jpn* 1996; 65: 2811-2823.
- 366 31. Ohtomo N, Tokiwano K, Tanaka Y, Sumi A, Terachi S, Konno H. Exponential
367 characteristics of power spectral densities caused by chaotic phenopmena. *J Phys Soc*
368 *Jpn* 1995; 64: 1104-1113.
- 369 32. Sumi A, Olsen LF, Ohtomo N, Tanaka Y, Sawamura S. Spectral study of measles
370 epidemics: the dependence of spectral gradient on the population size of the
371 community. *Jpn J Appl Phys* 2003; 42: 721-733.
- 372 33. Zaslavsky GM. *Chaos in Dynamic Systems*, Harwood Academic Publisers: London,
373 UK, 1985.

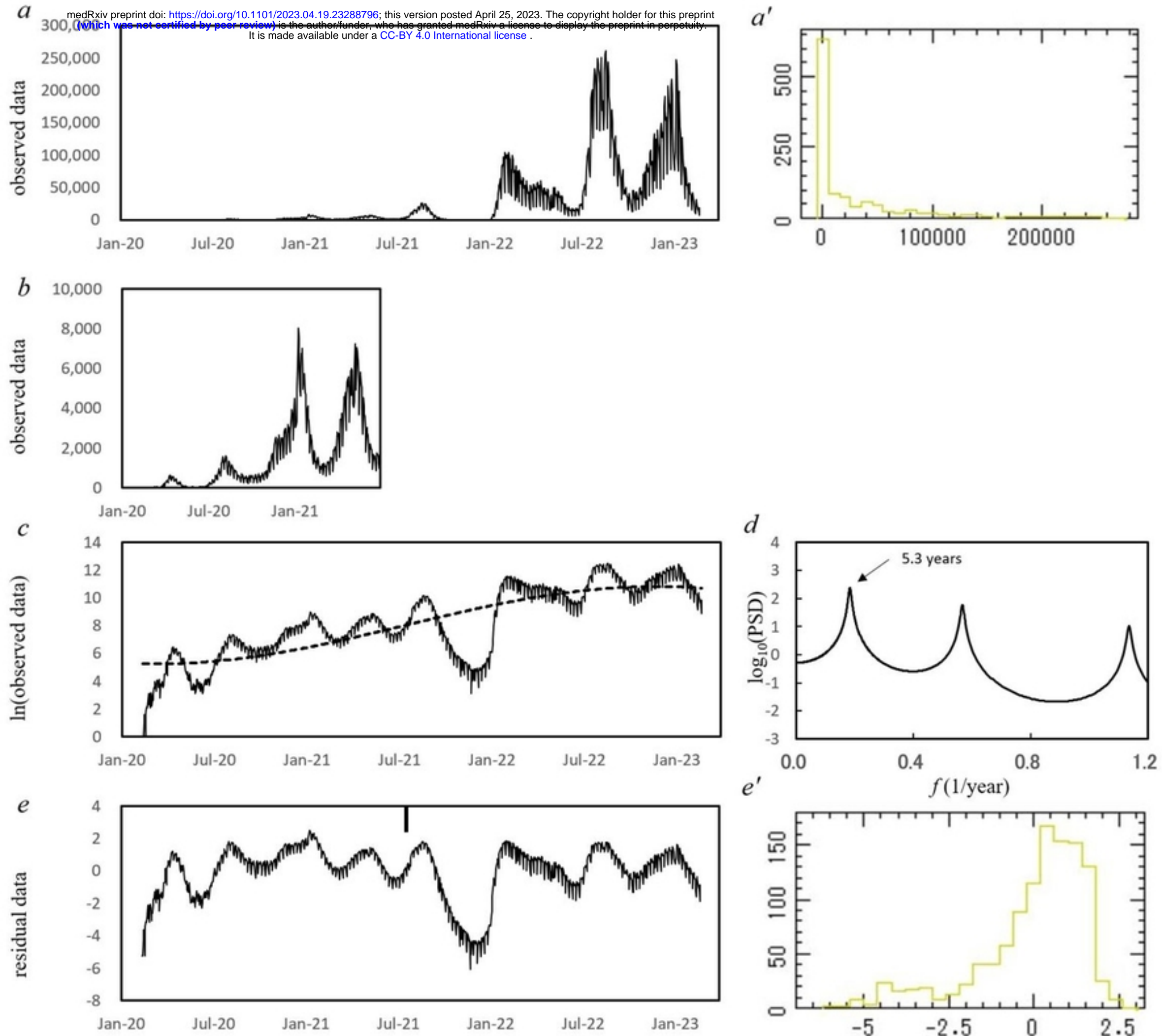


Fig 1

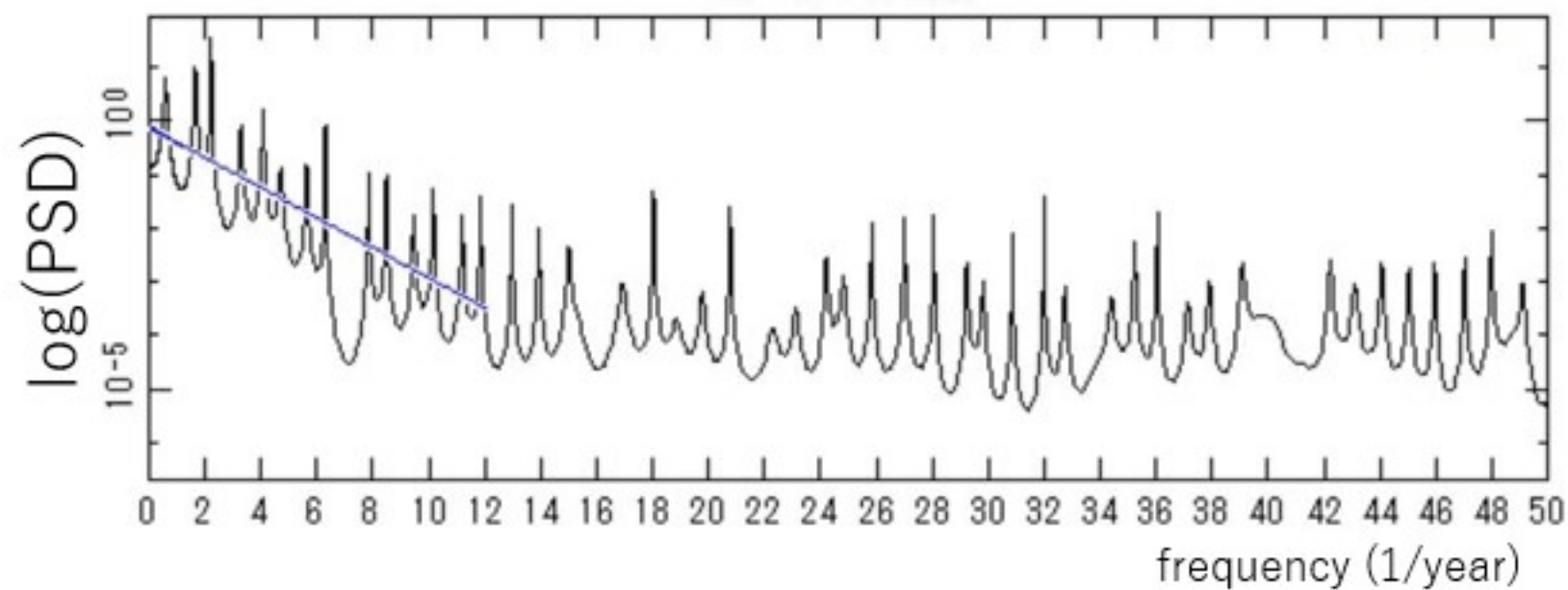
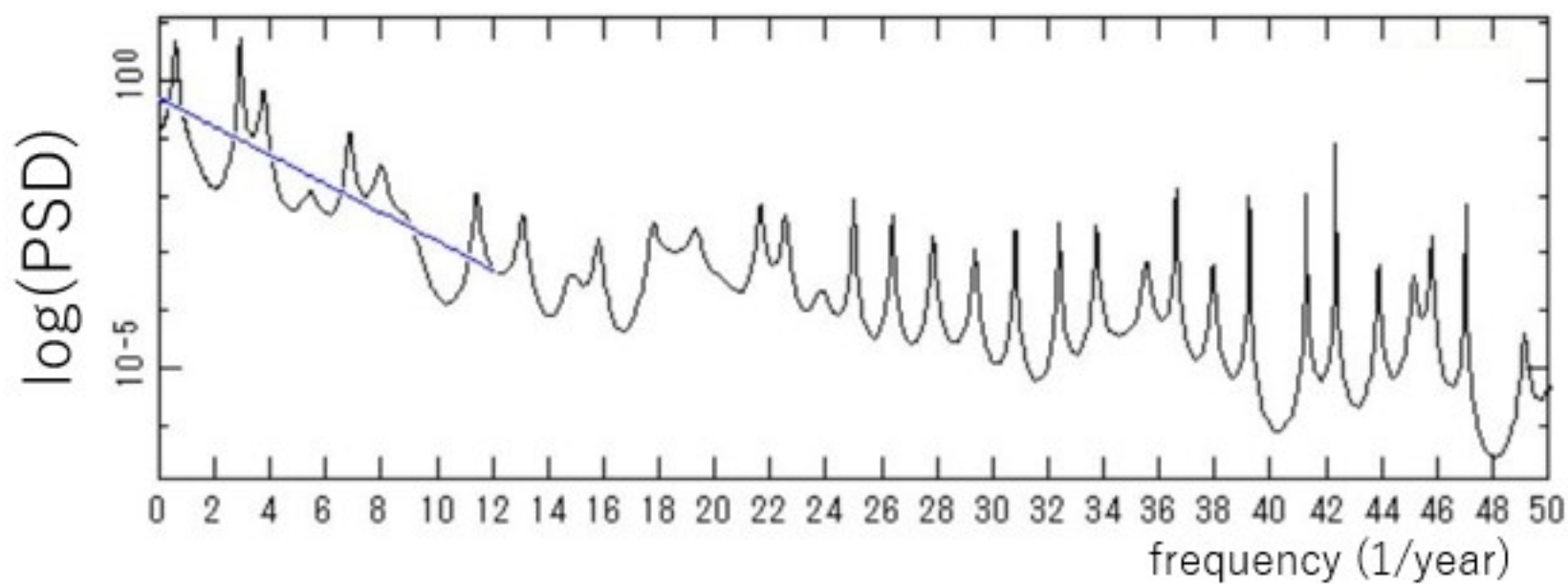


Fig 2

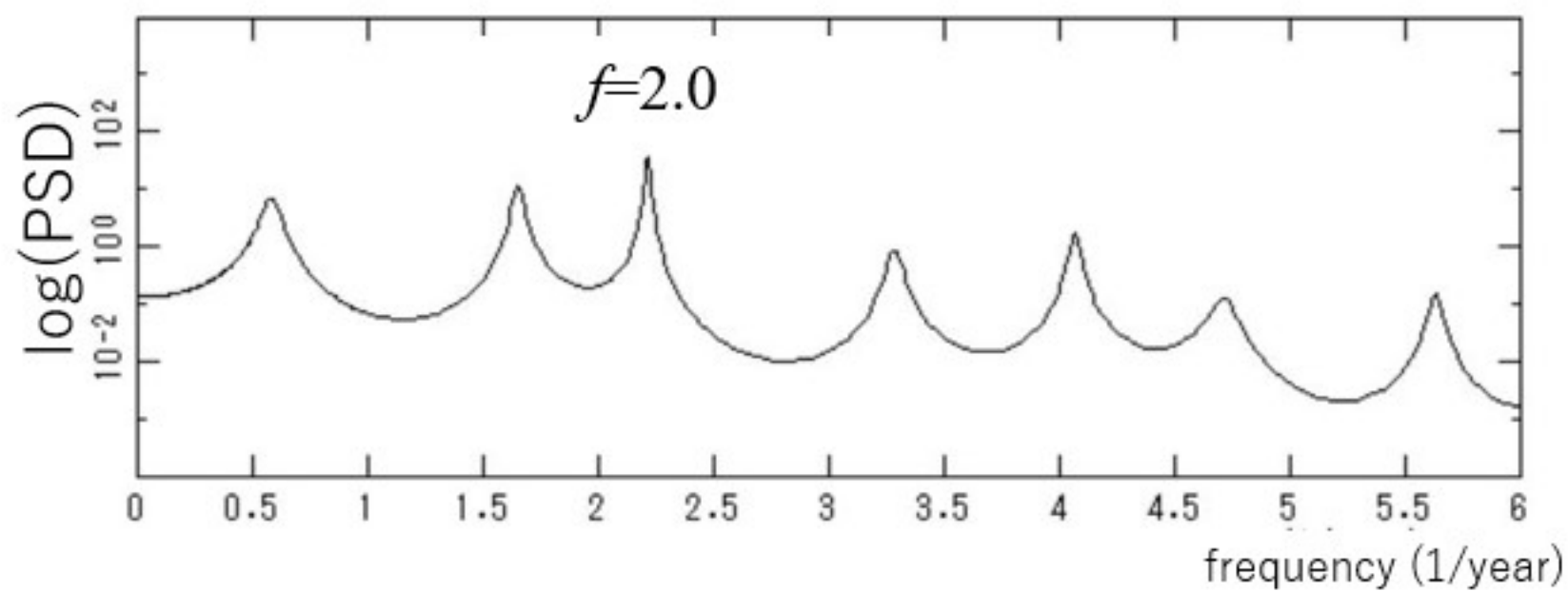
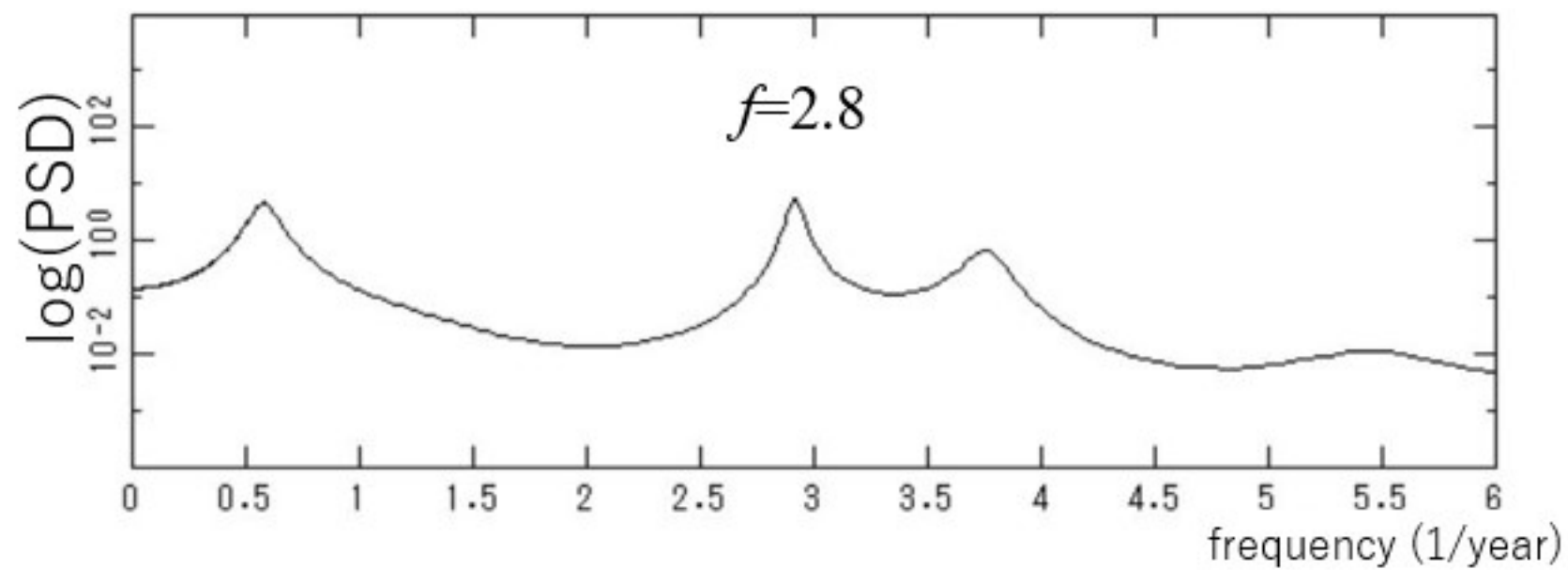


Fig 3

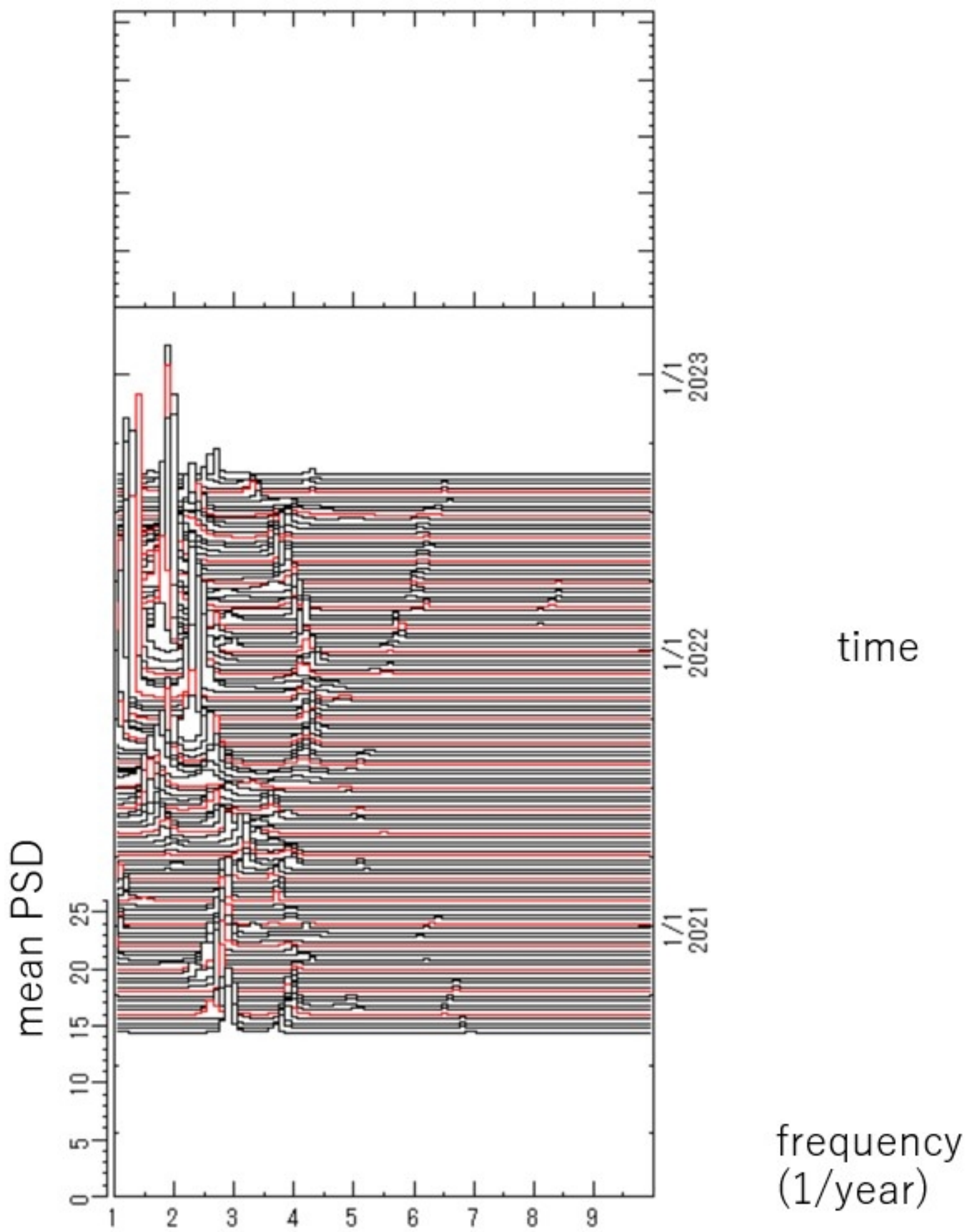


Fig 4

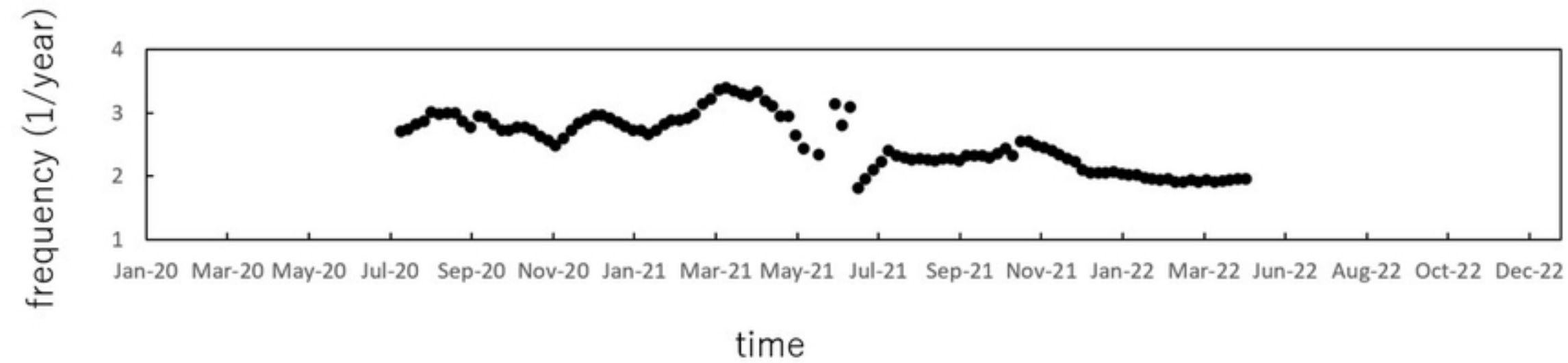


Fig 5